applied optics

Compact, low-cost, and broadband terahertz time-domain spectrometer

Nicolas Couture,[1] Jakob Schlosser,[1] Akif Ahmed,[2] Mamoun Wahbeh,[2] Garland Best,[2] Angela Gamouras,[1,3] and Jean-Michel Ménard[1,3,*]

[1]Department of Physics, University of Ottawa, Ottawa, Ontario K1N 6N5, Canada
[2]OZ Optics Limited, Ottawa, Ontario K0A 1L0, Canada
[3]National Research Council Canada, Ottawa, Ontario K1A 0R6, Canada
*jean-michel.menard@uottawa.ca

Received 15 February 2023; revised 23 April 2023; accepted 1 May 2023; posted 2 May 2023; published 18 May 2023

Terahertz time-domain spectroscopy (THz-TDS) is a powerful technique that enables the characterization of a large range of bulk materials, devices, and products. Although this technique has been increasingly used in research and industry, the standard THz-TDS configuration relying on the use of a near-infrared (NIR) laser source remains experimentally complex and relatively costly, impeding its availability to those without the expertise to build a high-performance setup based on nonlinear optics or without the financial means to acquire a commercial unit. Broadband THz-TDS systems require an even larger financial investment, primarily because the generation and detection of spectral components exceeding 3 THz typically need an ultrafast NIR source delivering sub-100-fs pulses. Such an ultrafast source can be bulky and cost upwards of $100,000. Here, we present a broadband, compact, and portable THz-TDS system comprising three modules that allow for the implementation of a single low-cost ultrafast laser, hence significantly decreasing the overall cost of the system. In the first module, the output laser pulses are spectrally broadened through nonlinear propagation in a polarization-maintaining optical fiber and then temporally compressed to achieve a higher peak power. The other two modules utilize thick nonlinear crystals with periodically patterned surfaces that diffract NIR pulses and optimize the efficiency of THz generation and detection processes by enabling a noncollinear beam geometry. Phase-matching conditions in the nonlinear crystals are controlled by the period of the gratings to gain access to a large spectral THz bandwidth. The whole system, combining these three modules, provides access to a THz spectrum peaking at 3.5 THz and extending beyond 6 THz with a maximum dynamic range of 50 dB for time-resolved spectroscopy applications. We demonstrate the functionality of this configuration by performing THz spectroscopy measurements of water vapor contained within a closed cell. Our compact system design paves the way towards a high-performance, yet cost-effective, THz-TDS system that can be readily used in academia and industry.

https://doi.org/10.1364/AO.486938

1. INTRODUCTION

The far-infrared region of the electromagnetic spectrum, broadly corresponding to optical wavelengths between 10 μm and 1000 μm and known as the terahertz (THz) band, is a rich area of research and development. THz radiation has a nonionizing photon energy offering new opportunities for noninvasive optical characterization of products and materials [1,2]. Notably, it is used to evaluate drug quality [3–5], detect structural flaws [6], identify organic and nonorganic contaminants in foods [7–9], and alert on the presence of bacteria and viruses [10–12]. These applications take advantage of unique properties of THz radiation: it can be transmitted through cardboards, polymers, and other materials opaque in the visible region. Additionally, THz radiation interacts with a large range of molecular vibrations, thereby enabling the detection and identification of many different compounds. THz time-domain spectroscopy (THz-TDS) is a characterization technique that relies on the generation and detection of phase-locked THz pulses. Compared to other optical characterization techniques that only record variations in optical intensity, THz-TDS has the advantage of extracting both amplitude and phase information of a THz pulse while mapping its full oscillating electric field. When a THz pulse is transmitted through or reflected at a surface, THz-TDS can directly extract the refractive index and absorption spectrum of that medium [2]. As THz spectroscopy and technologies offer such distinctive specifications, it complements, rather than competes with, other characterization techniques based on spectrometers, mass spectrometry, and Raman spectroscopy. Due to their scientific and practical significance, THz technologies and devices are in increasingly high demand and are a fast-growing research field in photonics.

Nonetheless, access to a broadband, sensitive, and affordable THz spectrometer is still a major hurdle to many applications in industrial, government, and academic laboratory settings. Some commercial THz-TDS systems that rely on photoconductive antennas (PCAs) feature a high dynamic range over a large spectral range, in part due to the ability to average over thousands of THz waveforms using rapid scanning methods such as asynchronous optical sampling [13]. THz systems employing PCAs typically have a peak sensitivity at frequencies below 1 THz [14], but can still reach, through averaging, an acceptable signal-to-noise ratio for particular spectroscopy applications at frequencies exceeding 4 THz. Other THz systems based on optical rectification in semiconductor crystals [15,16] can routinely generate and detect THz radiation at frequencies up to ∼3 THz. However, to generate higher THz frequency components, a near-infrared (NIR) laser source supporting a spectral bandwidth exceeding 3 THz is required. This condition corresponds to a < 100 fs pulse duration, which can only be delivered by high-end ultrafast systems. An alternative option to accessing broadband THz radiation consists of employing an independent optical module that broadens the laser spectrum in a nonlinear medium and recompresses the pulses with dispersion compensation optics [17,18]. We present such a module, consisting of a fiber and a chirped mirror pair, which significantly decreases the pulse duration while maintaining low-injection loss, hence boosting the peak field of the NIR laser pulses. Another major factor limiting the THz bandwidth is the nature and thickness of the crystals used for nonlinear generation and detection. Semiconductors such as ZnTe, GaAs, and $LiNbO_3$ have phase-matching conditions and phonon absorption tails preventing efficient THz generation above 3 THz. Previous work has demonstrated that a GaP crystal can be used to access larger THz frequencies [17], but a relatively thin crystal was required to achieve a broad THz bandwidth. Thick crystals are more desirable to increase THz generation and detection efficiencies since they enable long nonlinear interaction lengths. However, phase mismatch then becomes a dominant factor, and only those THz frequencies satisfying phase-matching conditions can be efficiently generated or detected. Here, we use surface phase gratings etched onto thick GaP crystals to overcome this limitation [19]. This configuration induces a tilted-pulse front inside the generation and detection crystals to increase the nonlinear interaction length while also providing access to a large THz spectral bandwidth [20,21]. The combination of the three modules allows the THz-TDS system to cover a large THz spectral bandwidth of >4 THz (FWHM) at a peak frequency of 3.5 THz. This THz-TDS system is, to our knowledge, unique in terms of its spectral properties combined with a simple and compact design. This article is ordered as follows: first, we demonstrate how the first module, referred to as the peak field booster (PFB), improves the performance of a fiber–laser source to yield suitable pulses to generate and detect broadband THz radiation. Then, we investigate the performance of the THz-TDS system employing GaP crystals with phase gratings on their surfaces by comparing to THz generation and detection results obtained with the same setup using standard nonpatterned GaP crystals. Finally, we demonstrate the functionality of our THz-TDS by performing spectroscopy of water vapor.

2. EXPERIMENT

A schematic of the THz-TDS scheme described in this work is shown in Fig. 1. To realize broadband THz-TDS, we employ a low-energy (5 nJ) femtosecond fiber laser oscillator delivering 130 fs pulses at a repetition rate of 40 MHz centered at a wavelength of 1064 nm (Ekspla FF200) and a PFB mounted directly onto the laser head. In a THz-TDS setup, spectral broadening of the incident NIR pulses allows the generation of higher THz frequencies, while temporal compression of these pulses ensures more efficient electro-optic sampling (EOS) detection [22]. Nonlinear propagation in a 10-cm-long polarization-maintaining fiber (PMF) with a 6 μm core diameter (OZ Optics PMF-980-6/125-0.25-L) broadens the NIR spectral bandwidth from 24 nm to 40 nm. As shown in Fig. 2(a), these bandwidths correspond to roughly 6 THz and 12 THz (FWHM) in optical frequency, respectively. Multiple reflections (14 in total) on the chirped mirror pair (CMP, Edmund Optics #12-328) provide a total group delay dispersion of -2800 fs^2 and compress the pulse from 130 fs to 50 fs [Fig. 2(b)]. This compression combined with a relatively high power transmission (78%) through the PFB yields an increase of the NIR pulse peak field by a factor of 2. A 1-mm-thick GaP crystal is used for THz generation, and a 2-mm-thick GaP crystal is used for detection through EOS. With a NIR wavelength of 1064 nm, phase-matching conditions and a second-order nonlinear process in a standard GaP window yield the production and detection of radiation at 1.5 THz [23,24]. Here, a phase grating is etched onto the surface of these two crystals via inductively coupled plasma

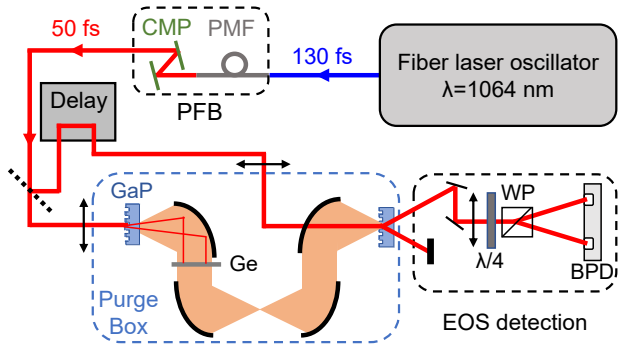

Fig. 1. Schematic of the compact and broadband THz-TDS system. A peak field booster (PFB) module, mounted to the output of a fiber laser oscillator (blue line), contains a polarization-maintaining fiber (PMF) to broaden the spectrum and a chirped mirror pair (CMP) to temporally compress the pulse. The output of the PFB is sent to a THz-TDS scheme relying on GaP crystals with phase gratings etched on their surfaces to generate and detect THz radiation. A germanium (Ge) wafer in the THz beam blocks the remaining NIR laser radiation after THz generation. THz detection is performed with electro-optic sampling (EOS) on one of the diffracted orders of the phase grating to achieve noncollinear phase matching and enhances sensitivity at frequencies >3 THz. This diffracted beam is collected with a periscope and then passed through a quarter-wave plate (λ/4) and Wollaston prism (WP) before being focused onto a pair of balanced photodiodes (BPDs) effectively monitoring the THz-induced change in polarization. The delay stage allows this process to be repeated for different temporal overlaps between the THz transient and the NIR pulse, allowing us to map out the full oscillating THz electric field via lock-in detection. A purge box filled with dry air removes atmospheric water vapor.

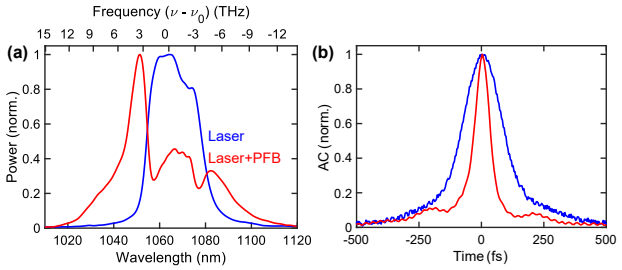

Fig. 2. (a) Spectra and (b) intensity autocorrelation (AC) traces of the pulses at the output of the ultrafast NIR source (blue line) and the PFB module (red line). The laser delivers 130 fs pulses carrying a 6 THz spectral bandwidth, which are spectrally broadened by the PFB to a 12 THz bandwidth and compressed to a 50 fs pulse duration. The high device throughput (only 22% loss in transmission) leads to an increase of the NIR pulse peak field by a factor of 2.

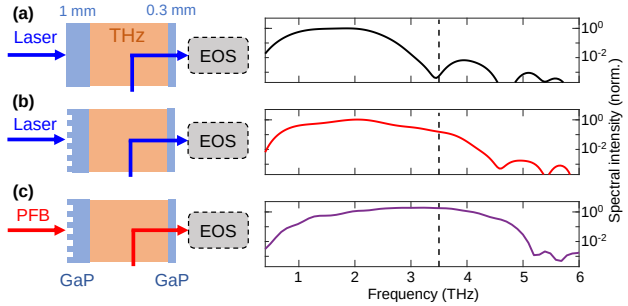

Fig. 3. Spectrum recorded by a THz-TDS system (plotted in log scale) using the direct laser output and (a) nonpatterned or (b) patterned 1-mm-thick GaP generation crystal. The grating on the surface of the generation crystal allows for nonlinear phase-matching conditions to be satisfied at higher THz frequencies, extending the spectrum beyond 4 THz. (c) THz spectrum measured with a setup incorporating both the PFB and the patterned 1-mm-thick GaP THz generation crystal. The spectrum extends beyond 5 THz, and the peak frequency shifts from 2 THz to 3.5 THz with the peak spectral intensity increasing by a factor of 2. In all three cases, the spectra are normalized to the maximum spectral intensity shown in (a), and a 0.3-mm-thick nonpatterned GaP crystal is used for detection to ensure a broadband detection window.

reactive ion etching, performed in-house, with a period of 1.635 μm corresponding to a 11.7° diffraction angle, allowing for noncollinear phase-matching conditions to be satisfied at 4 THz. The grating diffracts 85% of the incident NIR light in the first orders, whereas a mere 1.4% remains in the zeroth order, rendering the effect of the zeroth order NIR on the generated THz bandwidth negligible. Details related to the fabrication of the device are presented in [19]. This configuration mimics the titled-pulse-front generation scheme, commonly used for high-field THz generation in lithium niobate crystals [25–27], but without the complex beam geometry involving an external grating and a wedge-shaped nonlinear crystal. For EOS detection, a periscope collecting one of the grating diffraction orders is the only additional component needed when implementing a patterned detection crystal in the setup. Moreover, measuring one of the transmitted diffraction orders, instead of the zeroth order, leads to a polarization filtering effect at the back surface of the crystal resulting in an enhanced measurement sensitivity through a larger dynamic range [20,21]. The use of thick nonlinear crystals provides another advantage as it allows users to measure long EOS scanning ranges without recording parasitic THz echoes originating from multiple back reflections inside these crystals [28]. For the same reason, a thick (1 mm) Ge wafer is used as a spectral filter blocking the remaining NIR light after the THz generation crystal. As a result, an EOS scan of 30 ps can be performed before observing the first THz echo, yielding a spectral resolution of 33 GHz. The entire THz-TDS system, including the ultrafast source with the PFB, has the footprint of a $2' \times 3'$ optical breadboard and is mounted on a trolley for easy transportation. This proof-of-concept setup allows for additional design modifications for further miniaturization of the system.

3. RESULTS AND DISCUSSION

We first investigate how the PFB and THz generation crystal with the periodically patterned surface can be combined to achieve a broad THz spectrum. For this experiment, a standard thin 0.3-mm-thick GaP crystal is used for EOS detection to provide access to a large THz bandwidth as we study the effect of the laser spectral bandwidth and different types of THz generation crystals. The measurements performed with the reference setup, shown in Fig. 3(a), rely on laser output pulses directly impinging onto a 1-mm-thick nonpatterned THz generation crystal. The resulting THz spectrum extends up to 3 THz, peaks at ∼2 THz, and has a bandwidth of 2 THz (FWHM). In a second version of this setup, a patterned GaP crystal is used for THz generation, instead of the nonpatterned crystal with same thickness. In this case, the THz spectrum is extended beyond 4 THz and the bandwidth is increased to 3 THz (FWHM) [Fig. 3(b)]. After inserting the PFB immediately after the laser source [Fig. 3(c)], we observe spectral components extending beyond 5 THz, a peak frequency shifting from 2 to 3.5 THz, and a bandwidth exceeding 4 THz (FWHM).

Figure 4 shows the effect of replacing the 0.3 mm nonpatterned THz detection crystal by the 2-mm-thick crystal with a phase grating in a configuration that already combines the PFB and patterned THz generation crystal. In this case, we observe a larger field amplitude in the time-domain THz signal, by a factor of 6, resulting in an overall increase in detected spectral amplitude, especially around 3.5 THz. The phase gratings on the two nonlinear crystals diffract the NIR beam and allow noncollinear phase-matching conditions to be satisfied at 4 THz, which considerably improves both THz generation and detection processes around that frequency. Notably, the signal at lower THz frequencies is not significantly reduced as the corresponding wavelengths intrinsically have longer nonlinear coherence lengths. Furthermore, a polarization filtering effect at the back surface of the detection crystal enhances the THz detection sensitivity over the full spectrum by effectively reducing the optical noise on the photodiodes [20,21]. Combining the three modules, we achieve a spectrum reaching up to ∼ 6 THz, with the peak frequency at 3.5 THz and a spectral bandwidth of >4 THz. Figure 4(c) shows a dynamic range exceeding 50 dB at 3.5 THz, which is more than 20 dB higher than the value measured with a thin detection crystal (purple line). We evaluate the dynamic range of the system by dividing the intensity spectrum

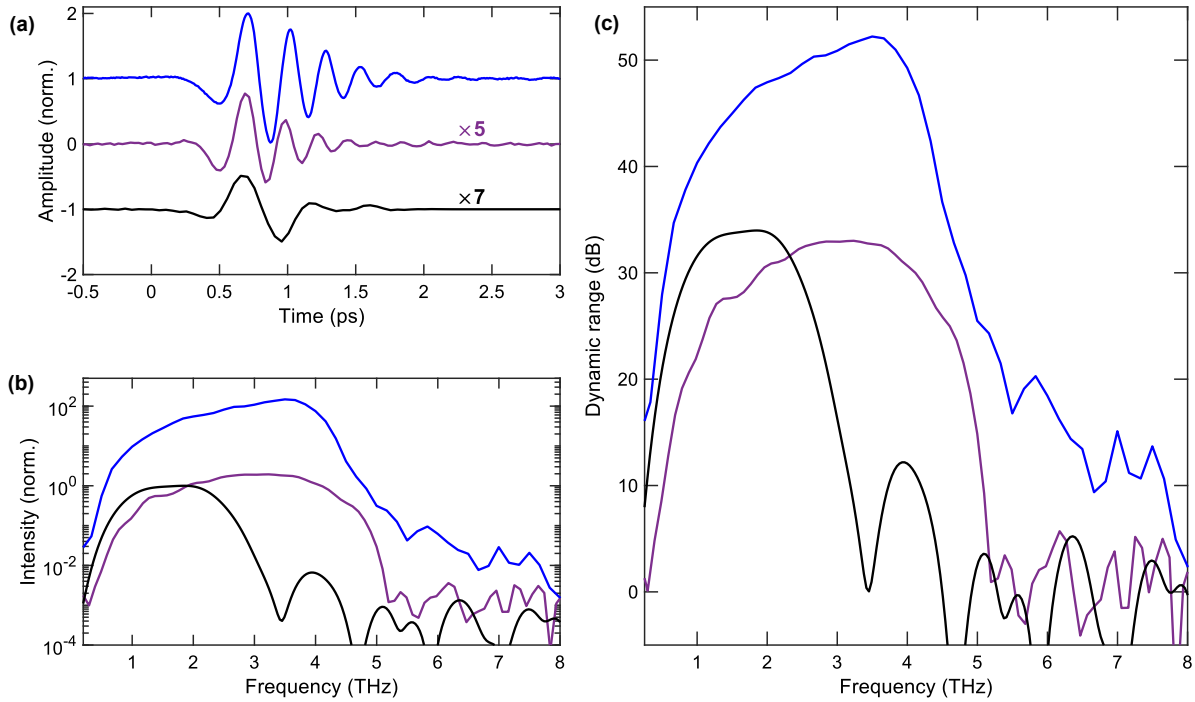

Fig. 4. (a) Time-domain signal and (b) spectral intensity measured with a setup using the PFB and the two thick patterned GaP crystals for THz generation (1 mm) and detection (2 mm) (blue line), a similar setup relying instead on a nonpatterned thin (0.3 mm) detection crystal (purple line), and a setup that is not relying on any of the three modules (black line). The spectral intensities are normalized to the peak of the black line. (c) Corresponding dynamic range achieved with each configuration.

by the noise floor. Our system's spectral coverage and sensitivity, related to its dynamic range, are comparable to those achieved with other THz-TDS systems relying on thin nonlinear crystals and a more complex optical source [29–31].

To demonstrate the spectroscopic capabilities of the system employing the three modules, time-resolved THz spectroscopy of a cell of water vapor is performed over a broad frequency range. The 3.8 cm by 2.5 cm by 2.5 cm cell has two external ports for gas injection and exhaust, and uses two input and output 10-μm-thick windows made of Zeonor, a cyclo olefin copolymer with high transparency in the THz region. The water vapor concentration is controlled and measured with a standard testing apparatus used to investigate gas sensing devices [32]. We achieve the desired concentration of water vapor in the cell by carefully adjusting the flow between two combined nitrogen gas lines, where one line is passed through a bubbler with water to reach a high vapor concentration. A reference THz time-domain waveform is recorded with a nitrogen-purged cell, allowing for the characterization of a cell containing 37% relative humidity (RH) [Fig. 5(a)]. These measurements were collected over a 30 ps time delay scanning range yielding a frequency resolution of 33 GHz. The corresponding measured absorption spectrum, which is in agreement with the transition intensity lines from the HITRAN database [33], is shown in Fig. 5.

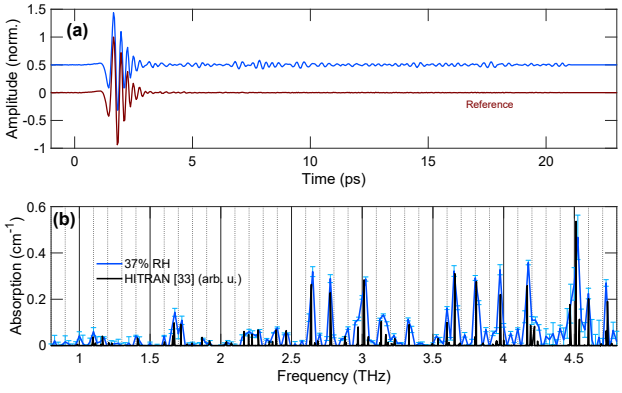

Fig. 5. (a) Recorded time-domain waveforms of the THz pulse passing through a 3.8-cm-long cell filled with water vapor at 37% RH (blue line), compared to a reference taken by purging the same cell with nitrogen (maroon line). The transients, normalized to the maximum field amplitude of the reference signal, are displayed with a vertical offset for clarity. In (b), the absorption spectrum of water vapor (blue line) is calculated from the Fourier transform of the waveforms in (a), possessing a frequency resolution of 33 GHz. Water vapor transition intensity lines (in arbitrary units) from the HITRAN database (black line) are superimposed on the experimental data. Error bars correspond to the standard deviation over three scans.

4. CONCLUSION

We demonstrate an easily transportable, broadband, and sensitive THz-TDS system relying on a cost-effective NIR source and a combination of three modules involving a PFB and two patterned nonlinear crystals. We show that the three respective components work together to ensure access to a broadband THz spectrum peaking at 3.5 THz and extending to a frequency range exceeding 6 THz. The system features a maximum dynamic range of 50 dB, which is approximately two orders of magnitude higher than a standard THz configuration relying

on the same laser source but without any of the three modules. Finally, the functionality of the system has been successfully tested for spectroscopic applications by performing broadband THz-TDS on a small volume of water vapor at 37% RH. Further technical development may still increase the measured dynamic range and scanning speed, potentially allowing our configuration to outperform THz characterization systems relying on high-end ultrafast laser systems. Our cost-effective and compact configuration is a major step towards enabling broader access to THz-TDS systems for broadband characterization of materials in research and manufacturing.

Funding. Natural Sciences and Engineering Research Council of Canada (ALLRP/556169-20); National Research Council Canada (JCEP).

Acknowledgment. The authors thank Wei Cui for insightful discussions. We acknowledge funding from the Natural Sciences and Engineering Research Council of Canada (NSERC) Alliance Program and Ontario Graduate Scholarship. We also acknowledge funding from the NRC-uOttawa Joint Centre for Extreme Photonics.

Disclosures. The authors declare no conflicts of interest.

Data availability. Data underlying the results presented in this paper are not publicly available at this time but may be obtained from the authors upon request.

REFERENCES

1. B. Ferguson and X.-C. Zhang, "Materials for terahertz science and technology," Nat. Mater. **1**, 26–33 (2002).
2. M. Tonouchi, "Cutting-edge terahertz technology," Nat. Photonics **1**, 97–105 (2007).
3. K. L. Nguyen, T. Friscić, G. M. Day, L. F. Gladden, and W. Jones, "Terahertz time-domain spectroscopy and the quantitative monitoring of mechanochemical cocrystal formation," Nat. Mater. **6**, 206–209 (2007).
4. J. A. Zeitler, P. F. Taday, D. A. Newnham, M. Pepper, K. C. Gordon, and T. Rades, "Terahertz pulsed spectroscopy and imaging in the pharmaceutical setting—a review," J. Pharm. Pharmacol. **59**, 209–223 (2007).
5. Y.-C. Shen, "Terahertz pulsed spectroscopy and imaging for pharmaceutical applications: a review," Int. J. Pharm. **417**, 48–60 (2011).
6. C. Jördens, M. Scheller, S. Wietzke, D. Romeike, C. Jansen, T. Zentgraf, K. Wiesauer, V. Reisecker, and M. Koch, "Terahertz spectroscopy to study the orientation of glass fibres in reinforced plastics," Compos. Sci. Technol. **70**, 472–477 (2010).
7. H. J. Shin, S.-W. Choi, and G. Ok, "Qualitative identification of food materials by complex refractive index mapping in the terahertz range," Food Chem. **245**, 282–288 (2018).
8. S. H. Baek, H. B. Lim, and H. S. Chun, "Detection of melamine in foods using terahertz time-domain spectroscopy," J. Agric. Food Chem. **62**, 5403–5407 (2014).
9. W. Liu, C. Liu, F. Chen, J. Yang, and L. Zheng, "Discrimination of transgenic soybean seeds by terahertz spectroscopy," Sci. Rep. **6**, 35799 (2016).
10. A. Mazhorova, A. Markov, A. Ng, R. Chinnappan, O. Skorobogata, M. Zourob, and M. Skorobogatiy, "Label-free bacteria detection using evanescent mode of a suspended core terahertz fiber," Opt. Express **20**, 5344–5355 (2012).
11. X. Yang, K. Yang, Y. Luo, and W. Fu, "Terahertz spectroscopy for bacterial detection: opportunities and challenges," Appl. Microbiol. Biotechnol. **100**, 5289–5299 (2016).
12. D.-K. Lee, J.-H. Kang, J. Kwon, J.-S. Lee, S. Lee, D. H. Woo, J. H. Kim, C.-S. Song, Q.-H. Park, and M. Seo, "Nano metamaterials for ultrasensitive Terahertz biosensing," Sci. Rep. **7**, 8146 (2017).
13. T. Yasui, E. Saneyoshi, and T. Araki, "Asynchronous optical sampling terahertz time-domain spectroscopy for ultrahigh spectral resolution and rapid data acquisition," Appl. Phys. Lett. **87**, 061101 (2005).
14. M. El Ghzaoui, S. Das, T. R. Lenka, and A. Biswas, eds., *Terahertz Wireless Communication Components and System Technologies* (Springer, 2022).
15. R. Huber, B. A. Schmid, R. A. Kaindl, and D. S. Chemla, "Femtosecond THz studies of intra-excitonic transitions," Phys. Status Solidi B **245**, 1041–1048 (2008).
16. A. Leitenstorfer, S. Hunsche, J. Shah, M. C. Nuss, and W. H. Knox, "Detectors and sources for ultrabroadband electro-optic sampling: experiment and theory," Appl. Phys. Lett. **74**, 1516–1518 (1999).
17. W. Cui, A. W. Schiff-Kearn, E. Zhang, N. Couture, F. Tani, D. Novoa, P. St.J. Russell, and J.-M. Ménard, "Broadband and tunable time-resolved THz system using argon-filled hollow-core photonic crystal fiber," APL Photon. **3**, 111301 (2018).
18. A. Halpin, N. Couture, and J.-M. Ménard, "Optical pulse structuring in gas-filled hollow-core kagomé PCF for generation and detection of phase-locked multi-THz pulses [Invited]," Opt. Mater. Express **9**, 3115–3122 (2019).
19. M. Bashirpour, W. Cui, A. Gamouras, and J.-M. Ménard, "Scalable fabrication of nanogratings on GaP for efficient diffraction of near-infrared pulses and enhanced terahertz generation by optical rectification," Crystals **12**, 684 (2022).
20. W. Cui, K. M. Awan, R. Huber, K. Dolgaleva, and J.-M. Ménard, "Broadband and high-sensitivity time-resolved THz system using grating-assisted tilted-pulse-front phase matching," Adv. Opt. Mater. **10**, 2101136 (2022).
21. A. Halpin, W. Cui, A. W. Schiff-Kearn, K. M. Awan, K. Dolgaleva, and J.-M. Ménard, "Enhanced terahertz detection efficiency via grating-assisted noncollinear electro-optic sampling," Phys. Rev. Appl. **12**, 031003 (2019).
22. A. Tomasino, A. Parisi, S. Stivala, P. Livreri, A. C. Cino, A. C. Busacca, M. Peccianti, and R. Morandotti, "Wideband THz time domain spectroscopy based on optical rectification and electro-optic sampling," Sci. Rep. **3**, 3116 (2013).
23. W. L. Bond, "Measurement of the refractive indices of several crystals," J. Appl. Phys. **36**, 1674–1677 (1965).
24. D. F. Parsons and P. D. Coleman, "Far infrared optical constants of gallium phosphide," Appl. Opt. **10**, 1683–1685 (1971).
25. J. Hebling, G. Almási, I. Z. Kozma, and J. Kuhl, "Velocity matching by pulse front tilting for large-area THz-pulse generation," Opt. Express **10**, 1161–1166 (2002).
26. J. Hebling, A. G. Stepanov, G. Almási, B. Bartal, and J. Kuhl, "Tunable THz pulse generation by optical rectification of ultrashort laser pulses with tilted pulse fronts," Appl. Phys. B **78**, 593–599 (2004).
27. A. G. Stepanov, J. Kuhl, I. Z. Kozma, E. Riedle, G. Almási, and J. Hebling, "Scaling up the energy of THz pulses created by optical rectification," Opt. Express **13**, 5762–5768 (2005).
28. F. Träger, *Springer Handbook of Lasers and Optics* (Springer, 2012).
29. K. Aoki, J. Savolainen, and M. Havenith, "Broadband terahertz pulse generation by optical rectification in GaP crystals," Appl. Phys. Lett. **110**, 201103 (2017).
30. C. Paradis, J. Drs, N. Modsching, O. Razskazovskaya, F. Meyer, C. Kränkel, C. J. Saraceno, V. J. Wittwer, and T. Südmeyer, "Broadband terahertz pulse generation driven by an ultrafast thin-disk laser oscillator," Opt. Express **26**, 26377–26384 (2018).
31. J. Drs, N. Modsching, C. Paradis, C. Kränkel, V. J. Wittwer, O. Razskazovskaya, and T. Südmeyer, "Optical rectification of ultrafast Yb lasers: pushing power and bandwidth of terahertz generation in GaP," J. Opt. Soc. Am. B **36**, 3039–3045 (2019).
32. R. Rautela, S. Scarfe, J.-M. Guay, P. Lazar, M. Pykal, S. Azimi, C. Grenapin, J. Boddison-Chouinard, A. Halpin, W. Wang, L. Andrzejewski, R. Plumadore, J. Park, J.-M. Ménard, M. Otyepka, and A. Luican-Mayer, "Mechanistic insight into the limiting factors of graphene-based environmental sensors," ACS Appl. Mater. Interfaces **12**, 39764–39771 (2020).
33. I. E. Gordon, L. S. Rothman, C. Hill, *et al.*, "The HITRAN2016 molecular spectroscopic database," J. Quant. Spectrosc. Radiat. Transf. **203**, 3–69 (2017).